

Multi-Agent DRL for Multi-Objective Twin Migration Routing with Workload Prediction in 6G-enabled IoV

Peng Yin, Wentao Liang, Jinbo Wen, Jiawen Kang, Junlong Chen, and Dusit Niyato, *Fellow, IEEE*

Abstract—Sixth Generation (6G)-enabled Internet of Vehicles (IoV) facilitates efficient data synchronization through ultra-fast bandwidth and high-density connectivity, enabling the emergence of Vehicle Twins (VTs). As highly accurate replicas of vehicles, VTs can support intelligent vehicular applications for occupants in 6G-enabled IoV. Thanks to the full coverage capability of 6G, resource-constrained vehicles can offload VTs to edge servers, such as roadside units, unmanned aerial vehicles, and satellites, utilizing their computing and storage resources for VT construction and updates. However, communication between vehicles and edge servers with limited coverage is prone to interruptions due to the dynamic mobility of vehicles. Consequently, VTs must be migrated among edge servers to maintain uninterrupted and high-quality services for users. In this paper, we introduce a VT migration framework in 6G-enabled IoV. Specifically, we first propose a Long Short-Term Memory (LSTM)-based Transformer model to accurately predict long-term workloads of edge servers for migration decision-making. Then, we propose a Dynamic Mask Multi-Agent Proximal Policy Optimization (DM-MAPPO) algorithm to identify optimal migration routes in the highly complex environment of 6G-enabled IoV. Finally, we develop a practical platform to validate the effectiveness of the proposed scheme using real datasets. Simulation results demonstrate that the proposed DM-MAPPO algorithm significantly reduces migration latency by 20.82% and packet loss by 75.07% compared with traditional deep reinforcement learning algorithms.

Index Terms—IoV, 6G, multi-objective VT migration, LSTM-based Transformer, DM-MAPPO.

I. INTRODUCTION

A. Background and Motivations

The Internet of Vehicles (IoV) enables network connections through vehicle-to-vehicle and vehicle-to-infrastructure communication, with mobile vehicles serving as information perception objects [1]. To enhance traffic operation efficiency, vehicles need to acquire real-time information from their surrounding environments and infrastructure through built-in wireless sensors. The Sixth-Generation (6G) wireless communication technology is anticipated to achieve ultra-reliable and low-latency communications with large-scale coverage [2],

supporting intelligent applications while meeting the reliability and security demands of future communication networks. With the adoption of 6G technology, the coverage and real-time performance of IoV will be significantly improved, encompassing connections across space, air, and ground [3]. In 6G-enabled IoV networks, edge servers, such as RoadSide Units (RSUs), Unmanned Aerial Vehicles (UAVs), and satellites, can deploy computationally intensive vehicular applications, including 3D virtual human remote projection, augmented reality navigation, and autonomous driving [4], providing users with immersive and high-quality vehicular services [5].

Vehicle Twins (VTs), functioning as an integrated Digital Twin (DT) technology, are high-precision virtual replicas of vehicles that combine physical vehicle models, sensing data, and historical data [6]. VTs play a crucial role in 6G-enabled IoV by collecting and analyzing traffic data to monitor vehicle states and predict traffic conditions [7]. However, constructing and updating VTs requires substantial computing and storage resources for real-time vehicle state monitoring and immersive service enhancement [8]. To address this, resource-constrained vehicles can offload VTs in the form of data packets to nearby edge servers (e.g., RSUs, UAVs, and satellites) after acquiring real-time data about themselves and their surroundings through multi-modal sensors, thus enabling more effective monitoring and simulation of vehicle states. Furthermore, with the support of 6G, vehicles can achieve reliable and ultra-low latency communications, ensuring real-time data updates and enhancing the responsiveness of vehicular applications.

Due to the dynamic mobility of vehicles and the uneven distribution of edge servers, the service range of a single edge server cannot fully cover the trajectory of vehicles in practical application scenarios. Thus, it is challenging to ensure long-term stable communication interaction between a moving vehicle and its static VTs. To maintain the continuity of high-quality vehicular applications and services, VTs need to be dynamically migrated among edge servers based on the driving route of the corresponding vehicle. However, implementing effective VT migration presents several challenges:

- **Challenges I. Nonuniform deployment of ground edge servers:** The distribution of ground edge servers (i.e., RSUs) varies significantly across different regions. For example, in cities, RSUs are densely deployed and generally follow a more regular distribution pattern. In contrast, rural areas generally have a sparse and scattered distribution of edge servers, which may disrupt the continuity of VT migration.

P. Yin is with the Defence Industry Secrecy Examination and Certification Center (e-mail: pedro_yin@163.com).

W. Liang, J. Kang, and J. Chen are with the School of Automation, Guangdong University of Technology, China (e-mails: WentaoL59@163.com; kavinkang@gdut.edu.cn; 3121001036@mail2.gdut.edu.cn).

J. Wen is with the College of Computer Science and Technology, Nanjing University of Aeronautics and Astronautics, China (e-mail: jinbo1608@nuaa.edu.cn).

D. Niyato is with the College of Computing and Data Science, Nanyang Technological University, Singapore (e-mail: dniyato@ntu.edu.sg).

Corresponding author: Jiawen Kang.

- **Challenge II. Dynamic workload of edge servers:** The mobility of vehicles, along with their spatial and temporal uncertainties, causes the workload of edge servers to fluctuate dynamically. Overloaded edge servers can hinder VT migration efficiency, compromising the quality of services provided to users. Therefore, it is necessary to accurately predict the workload of edge servers during VT migration.
- **Challenge III. Calculation complexity of VT migration decision-making:** Deep Reinforcement Learning (DRL) algorithms are widely recognized for their effectiveness in identifying optimal decision-making strategies [9]. However, traditional DRL algorithms may struggle to adapt to the complex and dynamic environment of VT migration, which may reduce the efficiency in identifying optimal VT migration routes.

B. Solutions and Contributions

To address these challenges, we propose a novel workload prediction-based VT migration framework in 6G-enabled IoV. Specifically, we introduce UAVs, leveraging their high mobility to complement RSU computing resources on busy roads during peak hours, and incorporate low-Earth orbit satellites to provide vehicular services in remote areas. To prevent VT migration interruptions during peak traffic hours, we propose a Long Short-Term Memory (LSTM)-based Transformer model to accurately predict the long-term workload of edge servers, thus avoiding VT migration to overloaded edge servers. Furthermore, considering the complex environment of 6G-enabled IoV involving simultaneous multiple VT migrations, it is difficult for traditional DRL algorithms to efficiently identify optimal VT migration routes. To overcome this limitation, we propose a Dynamic Mask Multi-Agent Proximal Policy Optimization (DM-MAPPO) algorithm. The DM-MAPPO algorithm dynamically determines whether all output actions meet the requirements and reduces the probability of unreachable actions to zero. Finally, the action sequence obtained by DM-MAPPO represents the most efficient VT migration route [10]. Our main contributions are summarized as follows:

- We propose a novel workload prediction-based VT migration framework in 6G-enabled IoV networks. This framework holistically incorporates RSUs, UAVs, and satellites as edge servers for VT migration, which can effectively address the problems of insufficient edge computing resources and low computing resource utilization in sparse regions (For Challenge I).
- To accurately predict the long-term workload of edge servers, we propose an LSTM-based Transformer model that introduces the LSTM module into the Transformer architecture. By leveraging the proposed LSTM-based Transformer model, the workload sequence of edge servers can be effectively predicted and utilized for VT migration decision-making, thereby avoiding temporary interruption in VT migration during peak traffic hours (For Challenge II).
- To efficiently obtain multiple optimal VT migration routes in the complex environment of 6G-enabled IoV

networks, we propose a DM-MAPPO algorithm. Specifically, we integrate a dynamic mask module into the MAPPO algorithm, which sets the output probability of each invalid action to 0, thereby dynamically reducing the action space and enhancing the efficiency of identifying optimal VT migration routes (For Challenge III).

The remainder of the paper is structured as follows: Section II provides a review of the relevant literature. Section III presents the workload prediction-based VT migration framework in 6G-enabled IoV networks. In Section IV, we formulate the optimization models for multiple VT migrations. In Section V, we propose the LSTM-based Transformer model to predict the workload of edge servers for VT migration. In Section VI, we propose the DM-MAPPO algorithm to identify multiple optimal VT migration routes. Section VII shows the simulation results of the proposed scheme. Finally, the paper is concluded in Section VIII.

II. RELATED WORK

A. VTs in 6G-enabled IoV

6G-enabled IoV is expected to become a key component of intelligent transportation systems [1], [11], [12]. In [1], the authors highlighted the necessity of upgrading communication technology to support latency-sensitive applications in IoV. In 6G-enabled IoV, VTs are typically deployed on edge servers with sufficient computing resources to meet the low-latency requirements of vehicular services [13]–[15]. To alleviate the problem of excessive computational overhead caused by frequent VT updates, the authors in [16] employed a double deep Q-network algorithm to make optimal offloading decisions. Similarly, in [17], the authors applied the deep deterministic policy gradient algorithm to deploy VTs on RSUs. In [8], the authors first predicted vehicle trajectories and utilized the Multi-Agent DRL (MADRL) algorithm to pre-migrate VTs to the target RSUs, thereby reducing the latency of subsequent VT migration. However, the above studies do not consider the uneven distribution of RSUs and the channel complexity of VT migration, which cannot guarantee the continuity of VT services. Therefore, it is necessary to introduce a new edge computing paradigm for VT migration in 6G-enabled IoV networks.

B. Workload Prediction of Edge Servers

To prevent VTs from being migrated to overloaded edge servers, it is essential to predict the long-term workload of edge servers in advance. In the field of time series prediction, the emergence of Recurrent Neural Networks (RNNs) has shown promise for long-term traffic flow forecasting [18]. Gated Recurrent Unit (GRU) and LSTM networks retain long-term memory through gating mechanisms and cell states, offering both effectiveness and lightweight properties [19], [20]. Based on the combination of graph neural networks and RNNs, the authors in [21] proposed a dynamic graph convolutional cycle network to improve traffic prediction accuracy by capturing dynamic correlation features between vehicle locations in the road network. In recent years, more prediction algorithms have been improved on the basis of

Transformers and carried out long-term time series prediction [22]. For instance, the authors in [23] proposed the Pyraformer algorithm, which captures multi-resolution features through an inter-scale tree structure. In [24], the authors proposed the Informer algorithm, which utilizes a prob-sparse self-attention mechanism with a distillation technique to efficiently extract key information. Due to the strong periodicity of traffic flow data, these algorithms generally focus on capturing long-term periodicity information while overlooking some short-term time series variations. However, edge servers are highly sensitive to fluctuations in traffic flow data, making accurate workload prediction crucial for efficient VT migration decisions.

C. MADRL for Routing Tasks

MADRL algorithms are powerful tools for obtaining optimal decision strategies in routing tasks, enabling collaborative task planning and multi-objective strategy optimization among DRL agents. In [25], the authors utilized collaborative MADRL algorithms to optimize routing policies, which demonstrates the advantages of MADRL in task planning and strategy optimization. Among various MADRL algorithms, MAPPO stands out as an efficient and stable optimization algorithm, which is widely utilized in routing tasks [26]. For example, the authors in [26] utilized the MAPPO algorithm to assign mobile policies to each UAV, thereby maximizing the service quality for ground equipment. In [27], the authors adopted the MAPPO algorithm to select edge service migration targets in the multi-reconfigurable intelligent surface-assisted vehicular edge computing network. However, the actions selected by MAPPO may not always comply with physical constraints. Specifically, some actions attempt to migrate VTs to edge servers that are either out of service or overloaded, potentially leading to vehicular service outages. In addition, the number of edge servers is positively correlated with the action space of MAPPO. As the number of edge servers increases, the likelihood of selecting invalid actions also grows. Moreover, the training time of MAPPO is closely related to the size of the action space. Notably, the authors in [28] proved that in environments with large action spaces, the operation of trying all possible actions at each step is redundant, deteriorating algorithm convergence and reducing the long-term rewards obtained. Since VT migration routing contains a large action space, it is necessary to design an efficient MADRL algorithm capable of identifying optimal VT migration routes.

III. SYSTEM MODEL

As shown in Fig. 1, we propose a workload prediction-based VT migration framework in 6G-enabled IoV networks, consisting of V vehicles, N RSUs, U UAVs, and one satellite. The framework is simulated over multiple time slots. In each time slot t , we denote the vehicle set and the RSU set as $\mathcal{V}^t = \{1, \dots, v, \dots, V\}$ and $\mathcal{N}_v^t = \{1, \dots, n_v^t, \dots, N\}$, respectively, where n_v^t represents the RSU n providing vehicular services to vehicle v in time slot t . The UAV set is denoted as $\mathcal{U}_v^t = \{1, \dots, u_v^t, \dots, U\}$, where u_v^t represents

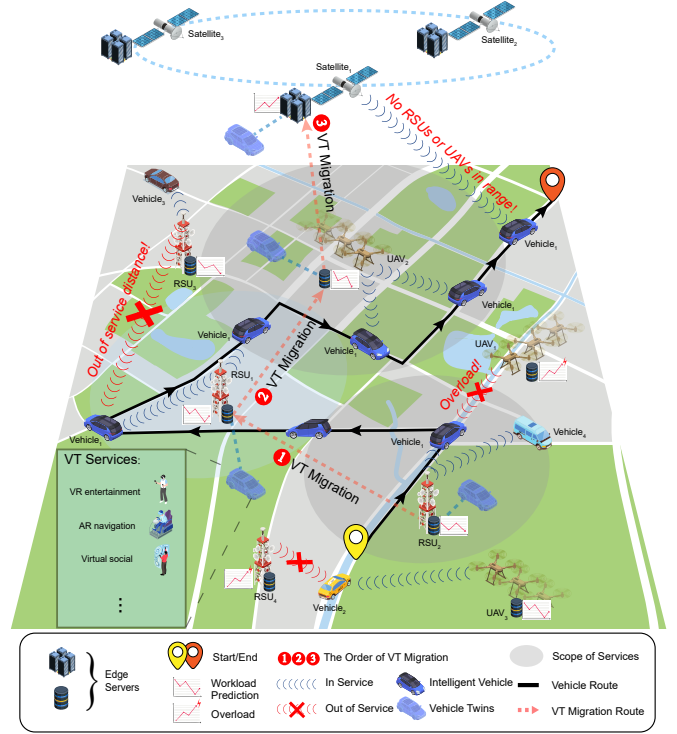


Fig. 1: The workload prediction-based VT migration framework in 6G-enabled IoV networks.

the UAV u serving vehicle v in time slot t . Additionally, we denote the satellite providing vehicle v in time slot t as s_v^t . Thus, the total number of edge servers in this framework is $M = N + U + 1$, where the edge server set is given by $\mathcal{M}_v^t = \mathcal{N}_v^t \cup \mathcal{U}_v^t \cup s_v^t = \{1, \dots, m_v^t, \dots, M\}$, including the RSU set, the UAV set, and the satellite. The maximum communication distance of edge server m is D_m^{max} , and the maximum cache size is L_m^{max} .

A. Network Model

In time slot t , the latitude and longitude of vehicle v are denoted as ϕ_v^t and λ_v^t , respectively, while the latitude and longitude of edge server m are represented as ϕ_m^t and λ_m^t , respectively. We denote the latitude difference between vehicle v and edge server m as $\Delta\phi_{v,m}^t = \frac{\pi}{180}(\phi_v^t - \phi_m^t)$, and the longitude difference as $\Delta\lambda_{v,m}^t = \frac{\pi}{180}(\lambda_v^t - \lambda_m^t)$. Based on the Haversine function, the central angular radian $\eta_{v,m}^t$ corresponding to the distance $D_{v,m}(t)$ between vehicle v and edge server m can be calculated as

$$\eta_{v,m}^t = 2 \arcsin \sqrt{\text{hav}(\eta_{v,m}^t)}, \quad (1)$$

where the Haversine function is $\text{hav}(\eta_{v,m}^t) = \sin^2\left(\frac{\eta_{v,m}^t}{2}\right) = \sin^2(\Delta\lambda_{v,m}^t) + \cos\left(\frac{\pi}{180}\phi_v^t\right)\cos\left(\frac{\pi}{180}\phi_m^t\right)\sin^2(\Delta\phi_{v,m}^t)$.

Considering the Earth's curvature and the altitude difference between UAVs and the ground, the distance $D_{v,m}(t)$ between vehicle v and edge server m in time slot t is given by

$$D_{v,m}(t) = \begin{cases} R \cdot \eta_{v,m}^t, & m \in \mathcal{N}_v^t, \\ \sqrt{(R \cdot \eta_{v,m}^t)^2 + h_u^2}, & m \in \mathcal{U}_v^t, \end{cases} \quad (2)$$

where h_u represents the cruise altitude of UAV u , and R represents the radius of the Earth, standing at 6,371.393 km. Similarly, the distance $D_{m,m_d}^{mig}(t)$ between edge server m and edge server $m_d \in \mathcal{M}_v^t$ can be calculated using Eq. (2) based on η_{m,m_d}^t , $m_d \in \mathcal{M}_v^t$.

Considering homogeneous channels between vehicles and edge servers, the gain of the Rayleigh fading channel between vehicle v and edge server m is given by [8]

$$h_{v,m}(t) = A \left(\frac{c}{4\pi f D_{v,m}(t)} \right)^2, \quad (3)$$

where $c = 3 \times 10^8$ m/s represents the speed of light, A represents the channel increment coefficient, and f represents the carrier frequency.

We consider that the orthogonal frequency division multiplexing access technology is applied in the proposed framework [29], indicating that the communication channels between different vehicles and an edge server are orthogonal. Based on Eq. (3), the uplink transmission speed between vehicle v and edge server m can be calculated as [30]

$$R_{v,m}^{up}(t) = B_m^{up} \log \left(1 + \frac{p_v h_{v,m}(t)}{\sigma^2} \right), \quad (4)$$

where σ represents the additive white Gaussian noise, p_v represents the transmit power of vehicle v , and B_m^{up} represents the uplink bandwidth.

Similarly, the downlink transmission speed between vehicle v and edge server m can be calculated as

$$R_{v,m}^{down}(t) = B_m^{down} \log \left(1 + \frac{p_m h_{v,m}(t)}{\sigma^2} \right), \quad (5)$$

where p_m represents the signal transmission power of edge server m , and B_m^{down} represents the downlink bandwidth.

Satellites are generally considered to be in geosynchronous orbit at 35,786km above the Earth's surface, while low-Earth-orbit satellites typically operate at an altitude of 550 km. In each time slot, the size of the data generated by vehicle v , including VT migration requests, is denoted as S_v . Based on the uplink transmission speed, the uplink latency $T_{v,m}^{up}(t)$ is given by

$$T_{v,m}^{up}(t) = \begin{cases} \frac{S_v}{R_{v,m}^{up}(t)}, & m \neq s_v^t, \\ \frac{S_v}{R^{SAT}}, & m = s_v^t, \end{cases} \quad (6)$$

where R^{SAT} is the Starlink data transmission speed¹. Similarly, the downlink latency $T_{v,m}^{down}(t)$ can be calculated as

$$T_{v,m}^{down}(t) = \begin{cases} \frac{S_v}{R_{v,m}^{down}(t)}, & m \neq s_v^t, \\ \frac{S_v}{R^{SAT}}, & m = s_v^t. \end{cases} \quad (7)$$

¹Data from Starlink website: <https://www.starlink.com/technology>

B. Computing Model

We define the size of pending data in the cache of the edge server m in time slot t as $S_m(t)$. Thus, the load of edge server m in time slot t can be calculated as

$$S'_m(t) = S_m(t) + \sum_{v=1}^V g_{v,k} S_v, \quad (8a)$$

$$g_{v,k} = \begin{cases} 0, & k \neq m^t, \\ 1, & k = m^t, \end{cases} \quad (8b)$$

where $g_{v,k} = 1$ indicates that vehicle v is served by edge server m , otherwise $g_{v,k} = 0$. When the amount of data to be processed by the edge server m in time slot t becomes too large, it may cause data packet dropout during VT migration, affecting the vehicular services provided by VTs to users. If RSUs or UAVs become overloaded, the VTs need to be offloaded to the satellite to obtain additional computing resources, albeit at a higher cost. Thus, the computing latency is given by [31]

$$T_{v,m}^{cul}(t) = \begin{cases} \frac{e_v S'_m(t)}{C_m}, & S'_m(t) \leq L_m^{max}, \\ \frac{e_v S'_m(t)}{C_s}, & S'_m(t) > L_m^{max}, \end{cases} \quad (9)$$

where e_v represents the number of computation cycles required per bit, C_m denotes the Central Processing Unit (CPU) operating frequency of edge server m , $m \neq s_v^t$, and C_s denotes the CPU operating frequency of the satellite.

C. Migration Model

In this framework, VTs need to be migrated among edge servers to ensure short-distance communication with vehicles. However, VT migration will increase the workload of edge servers, leading to problems such as time alignment, resource waste, and service interruption. If VT migration occurs at edge server m , the state of edge server m in time slot t will be different from the state of time slot $t+1$. Thus, whether VT migration can occur at edge server m can be judged by

$$J_m^t = \begin{cases} 1, & m^t \neq m^{t+1}, \\ 0, & m^t = m^{t+1}. \end{cases} \quad (10)$$

After edge server m receives a VT migration request from vehicle v , the VTs of vehicle v are migrated from the originally connected edge server m to the target edge server m_d , and the migration transmission speed can be calculated as

$$R_{m,m_d}^{mig}(t) = B_{m,m_d}^{mig} \log \left(1 + \frac{p_m h_{m,m_d}^{mig}(t)}{\sigma^2} \right), \quad (11)$$

where B_{m,m_d}^{mig} represents the migration transmission bandwidth, p_m represents the transmit power of edge server m , and $h_{m,m_d}^{mig}(t) = A \left(\frac{c}{4\pi f D_{m,m_d}^{mig}(t)} \right)^2$.

Based on Eq. (10) and Eq. (11), the cost of VT migration can be quantified as the transmission latency $T_{v,m,m_d}^{mig}(t)$ between edge server m and edge server m_d , given by [8]

$$T_{v,m,m_d}^{mig}(t) = J_m^t \frac{S_v^{mig}}{R_{m,m_d}^{mig}(t)}, \quad (12)$$

where S_v^{mig} represents the size of migrated VT data corresponding to the vehicle v .

Thus, the total latency $T_{v,m}^{sum}(t)$ of VT migration from edge server m to edge server m_d is given by

$$T_{v,m}^{sum}(t) = T_{v,m}^{up}(t) + T_{v,m}^{down}(t) + T_{v,m}^{cul}(t) + T_{v,m,m_d}^{mig}(t). \quad (13)$$

If vehicle v is out of the service range of the connected edge server m , or the connected edge server m is overloaded, the corresponding VT migration will fail. Thus, whether the VT migration of vehicle v fails in time slot t is given by

$$\xi_v^t = \begin{cases} 1, & D_{v,m}(t) > D_m^{max} \text{ or } S'_m(t) > L_m^{max}, \\ 0, & \text{otherwise,} \end{cases} \quad (14)$$

where $\xi_v^t = 1$ means that the VT migration of vehicle v fails.

In addition, vehicle v begins driving in time slot $t = 0$ and reaches its destination in time slot t_v^{end} . Based on Eq. (14), the packet loss rate during VT migration of vehicle v is denoted as the ratio of the number of packet losses to the total number of time slots, which can be calculated as

$$q_v = \frac{\sum_{t=0}^{t_v^{end}} \xi_v^t}{t_v^{end}} \times 100\%. \quad (15)$$

IV. PROBLEM FORMULATION

In this paper, we aim to optimize three objectives. The first goal is to minimize the total latency $T_{v,m}^{sum}(t)$ of all vehicles, thus ensuring a fully immersive experience. Secondly, the uneven distribution of RSUs in a region may cause cyclical and regional load peaks of edge servers. To balance the workload of all edge servers in the region, we take the variance of the workload of all edge servers $\text{Var}(S'_m(t))$ as one of the optimization objectives, and $\text{Var}(S'_m(t))$ can be calculated as $\text{Var}(S'_m(t)) = \sum_{i=1}^M (S'_i(t) - \mu_i(t))^2$, where $\mu_i(t)$ represents the average of $S'_m(t)$. Finally, frequent VT migrations not only lead to additional unnecessary computing overhead but also degrade the quality of vehicular services. Thus, the goal is to minimize the total number of VT migrations after optimization, and the three optimization objectives along with their corresponding constraints are formulated as

$$\min O_T = \sum_{v=1}^V \sum_{t=0}^{t_v^{end}} T_{v,m}^{sum}(t), \quad (16a)$$

$$\min O_V = \sum_{t=0}^{t_v^{end}} \text{Var}(S'_m(t)), \quad (16b)$$

$$\min O_D = \sum_{v=1}^V q_v, \quad (16c)$$

$$\text{s.t. } S'_m(t) \leq L_m^{max}, \quad (16d)$$

$$D_{v,m}(t) \leq D_m^{max}, \quad (16e)$$

$$m \in \mathcal{M}_v^t, \quad (16f)$$

where O_T represents the total latency, O_V represents the total workload variance, and O_D represents the total packet loss rate. Constraint (16d) is set to prevent packet loss or disconnection when VT data sent to the edge server m exceeds the maximum cache. Constraint (16e) is set to prevent

connected edge servers from going out of communication range. Constraint (16f) is set to prevent connections to edge servers that are not in the region.

Accurate workload data is crucial for VT migration planning tasks. Due to the large number of VT migration targets and the high communication and computing resource requirements of VT tasks, a large prediction error will lead to the failure of VT migration performed by the DRL algorithm, reducing the quality of the overall VT migration route.

V. LSTM-BASED TRANSFORMER MODEL FOR WORKLOAD PREDICTIONS OF EDGE SERVERS

The workload of edge servers often exhibits periodic patterns [32]. LSTM typically performs well in predicting periodic data [33], but it performs poorly for aperiodic data, especially in capturing fine-grained workload variations. In contrast, the Transformer model can effectively capture the relationships among vectors, making it a key technique for generating accurate contextual semantics in natural language processing [34]. In this section, we propose the LSTM-based Transformer model to predict the workload of edge servers. The structure of the proposed model is shown in Fig. 2.

The input time-series workload data² with length T is first processed through each LSTM module to capture the long-term cycle dependency of each edge server. Then, the output of each LSTM module $\mathbf{H}_t = [h_t, h_{t+1}, \dots, h_{t+T}]$ will be transformed into data with shape $T \times d_k$ through the Dense layer, where d_k represents the vector dimension used by the query and key vectors in the self-attention mechanism. Finally, the processed data is utilized as input to the Transformer module to predict the workload data of edge servers accurately. The prediction result will be mapped to the corresponding edge server, and the amount of data accumulated in the cache of the edge server will be calculated. The structure of the LSTM module is given by [35]

$$i_t = \sigma(x_t \mathbf{W}_x^i + h_{t-1} \mathbf{W}_h^i + \mathbf{b}_i), \quad (17a)$$

$$f_t = \sigma(x_t \mathbf{W}_x^f + h_{t-1} \mathbf{W}_h^f + \mathbf{b}_f), \quad (17b)$$

$$o_t = \sigma(x_t \mathbf{W}_x^o + h_{t-1} \mathbf{W}_h^o + \mathbf{b}_o), \quad (17c)$$

$$\widetilde{C}_t = \tanh(x_t \mathbf{W}_x^c + h_{t-1} \mathbf{W}_h^c + \mathbf{b}_c), \quad (17d)$$

$$C_t = \sigma(f_t \cdot C_{t-1} + i_t \cdot \widetilde{C}_t), \quad (17e)$$

$$h_t = o_t \cdot \tanh(C_t), \quad (17f)$$

where i_t represents the output of the input gate, f_t represents the output of the forget gate, o_t represents the output of the output gate, h_t represents the hidden state, C_t represents the cell state, \widetilde{C}_t represents the candidate cell state, \mathbf{W}_h^i , \mathbf{W}_h^f , \mathbf{W}_h^o , \mathbf{W}_h^c , \mathbf{W}_x^i , \mathbf{W}_x^f , \mathbf{W}_x^o , and \mathbf{W}_x^c represent the weight matrices of gates, and \mathbf{b}_i , \mathbf{b}_f , \mathbf{b}_o , and \mathbf{b}_c represent the bias term of gates.

The Transformer module employs the multi-head attention mechanism to process the input data. \mathbf{Q}_t^h , \mathbf{K}_t^h , and \mathbf{V}_t^h

²RSU coordinate dataset: <https://pems.dot.ca.gov/>

Algorithm 1: LSTM-based Transformer Model

Input: The sequence of traffic flow data X_m .

Output: Model_m, the MSE loss L_m of Model_m, predicted workload sequences of each edge server m .

- 1 **Phase 1: Initialization**
 - 2 Initialize the traffic flow prediction model Model_m.
The data X_m are preprocessed as
 $S_m(t), \dots, S_m(t+T) \rightarrow S_m(t+T+1)$.
 - 3 **Phase 2: Training**
 - 4 **for** $t = 0, 1, \dots, t_{end} - T$ **do**
 - 5 Input historical traffic flow data
 $X'_m = [S_m(t), \dots, S_m(t+T)]$.
 - 6 Obtain predicted traffic flow data $S_m^{pre}(t+T+1)$.
 - 7 Calculate the MSE loss
 $L_m = (S_m^{pre}(t+T+1) - S_m(t+T+1))^2$.
 - 8 **end**
 - 9 **Phase 3: Evaluation**
 - 10 Input historical traffic flow data X'_m into the trained traffic flow prediction model Model_m.
 - 11 Obtain predicted traffic flow data $S_m^{pre}(t+T+1)$ through Model_m.
 - 12 Calculate the accuracy rate
 $Acc_m = S_m^{pre}(t+T+1) - S_m(t+T+1)$ for each edge server.
 - 13 **for** $m = 1, 2, \dots, M - 1$ **do**
 - 14 Deploying the trained model Model_m to the edge server m .
 - 15 Input historical traffic flow data X'_m into edge server m to obtain the predicted traffic flow data $S_m^{pre}(t)$.
 - 16 Calculate the predicted workload of edge server m as $S'_m(t) = S_m(t) + S_v$, $m = m_v^t$.
 - 17 **end**
-

represent the query, key, and value vectors, respectively. Thus, the structure of the Transformer module is given by [34]

$$\mathbf{Q}_t^h = \mathbf{H}_t \mathbf{W}_Q, \quad (18a)$$

$$\mathbf{K}_t^h = \mathbf{H}_t \mathbf{W}_K, \quad (18b)$$

$$\mathbf{V}_t^h = \mathbf{H}_t \mathbf{W}_V, \quad (18c)$$

$$\text{head}_h = \text{softmax} \left(\frac{\mathbf{Q}_t^h \mathbf{K}_t^{hT}}{\sqrt{d_k}} \right), \quad (18d)$$

$$\text{Output} = \text{Concat}(\text{head}_1, \dots, \text{head}_1) \mathbf{W}_O, \quad (18e)$$

where \mathbf{W}_Q , \mathbf{W}_K , \mathbf{W}_V , and \mathbf{W}_O represent the trainable parameter matrices.

The output of the Transformer module represents the traffic flow $c_m(t)$ of each edge server, which can be mapped to the workload data of each edge server through $S_m(t) = S_v \cdot c_m(t)$. Algorithm 1 presents the pseudocode of the LSTM-based Transformer model, whose computational complexity is $\mathcal{O}(T \times M \times (H \times T^2 \times d_k + T \times d_h))$, where H denotes the number of attention heads, and d_h denotes the hidden dimension of each LSTM module. By leveraging the proposed LSTM-based Transformer model, VTs can avoid being migrated to

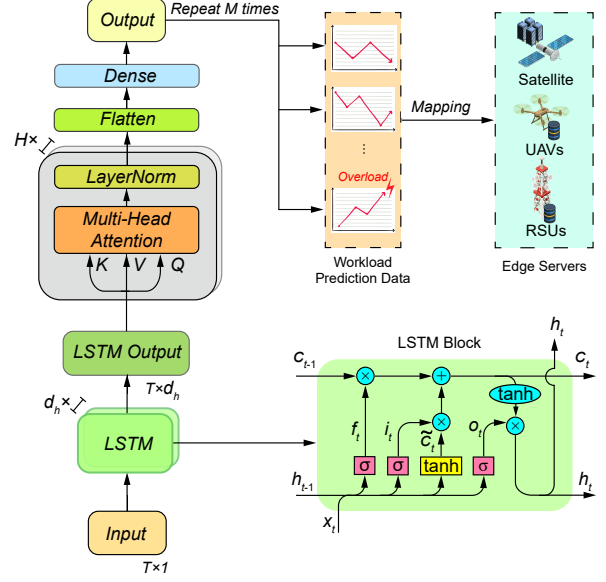


Fig. 2: The structure of the LSTM-based Transformer model.

overloaded edge servers. Similar to the traveling salesman problem [36], the formulated problem (16) is NP-hard, with a time complexity of $\mathcal{O}(n^n)$, making it nearly impossible to find the optimal solution through enumeration within a finite time. Fortunately, DRL algorithms provide solutions to NP-hard problems. However, traditional DRL algorithms suffer from long training times, leading to low efficiency and suboptimal solutions. Thus, we propose the DM-MAPPO algorithm to effectively solve the problem (16).

VI. DM-MAPPO ALGORITHMS FOR OPTIMAL VT MIGRATION ROUTES

In this section, we first model the VT migration routing task as a Partially Observable Markov Decision Process (POMDP). Then, we introduce the DM-MAPPO algorithm.

A. POMDP for VT Migration Routing Tasks

- **Observation Space:** During VT migration, vehicles can observe real-time information from the surrounding environment. The distance set of vehicle v from edge servers is denoted as $\mathbf{D}_v^o(t) = \{D_{v,1}(t), \dots, D_{v,m}(t), \dots, D_{v,M-1}(t)\}$. In this framework, the number of satellites is 1, and the communication distance and transmission rate have been determined. Thus, the distance between the satellite and the vehicle is not added to the observation set. The workload prediction set is denoted as $\mathbf{S}^o(t) = \{S_1^{pre}(t), \dots, S_m^{pre}(t), \dots, S_M^{pre}(t)\}$. For vehicle v , its observation in time slot t is denoted as

$$\mathbf{o}_v^t = [\mathbf{D}_v^o(t), \mathbf{S}^o(t)]. \quad (19)$$

Remarkably, all vehicles in the same area observe $\mathbf{S}^o(t)$ in a shared way.

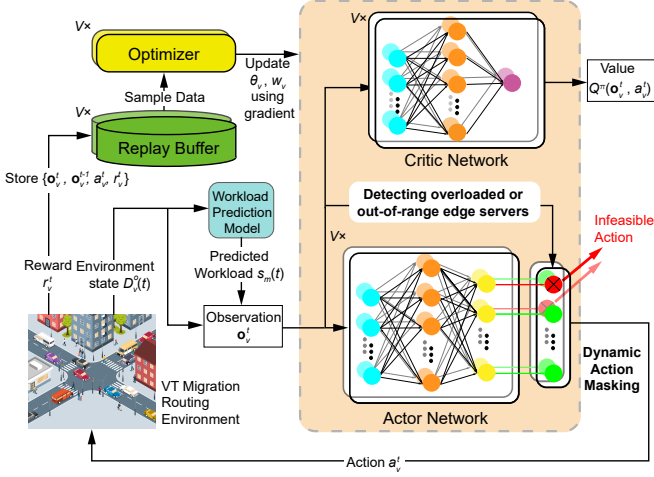


Fig. 3: The algorithm architecture of DM-MAPPO for optimal VT migration routes.

- **Action Space:** The action of each DRL agent is to select the edge server that provides vehicular services for vehicle v in time slot t . Thus, the action space can be denoted as $\mathcal{A}_v^t = [a_{v,1}^t, \dots, a_{v,m}^t, \dots, a_{v,M}^t]$, where $a_{v,m}^t$ presents that the DRL agent migrates VTs of vehicle v to edge server m . Beside, we denote the actor network output for each DRL agent as $\mathbf{P}_v^t = [P_{v,1}^t, \dots, P_{v,m}^t, \dots, P_{v,M}^t]$, where $\sum_{i=1}^M P_{v,i}^t = 1$. Finally, we perform the action a_v^t with the maximum probability as

$$a_v^t = \underset{m}{\operatorname{argmax}}(\mathbf{P}_v^t). \quad (20)$$

Since VTs can only exist on one edge server in each time slot t , the sampled action a_v^t is one-dimensional.

- **Immediate Reward:** The weighted summation method is utilized to transform the multi-objective optimization problem (16) into a single-objective optimization problem. After the objectives are normalized, the weighted summation is carried out, and the immediate reward is defined as

$$r_v^t(\mathbf{o}_v^t, a_v^t) = -(w_T \cdot \tilde{T}_{v,m}^{sum}(t) + w_s \cdot \widetilde{\operatorname{Var}}(\mathbf{S}^o(t)) + w_d \cdot \xi_v^t), \quad (21)$$

where w_T , w_s , and w_d represent the weights of optimization objectives, $\tilde{T}_{v,m}^{sum}(t)$ represents the latency $T_{v,m}^{sum}(t)$ after Z-score normalization in the time dimension, and $\widetilde{\operatorname{Var}}(\mathbf{S}^o(t))$ represents the workload variance after Z-score normalization in the time dimension.

- **Reward Shaping:** Reward shaping is an effective method to incorporate human knowledge into DRL agents [37]. To speed up the model training and convergence, we use the reward shaping method to guide DRL agents in identifying optimal VT migration routes. Specifically, the nonlinearity of variance makes it difficult for agents to improve the variance reward. Therefore, we replace the variance term $\widetilde{\operatorname{Var}}(\mathbf{S}^o(t))$ in Eq. (21) with $\tilde{S}_m(t)$, and

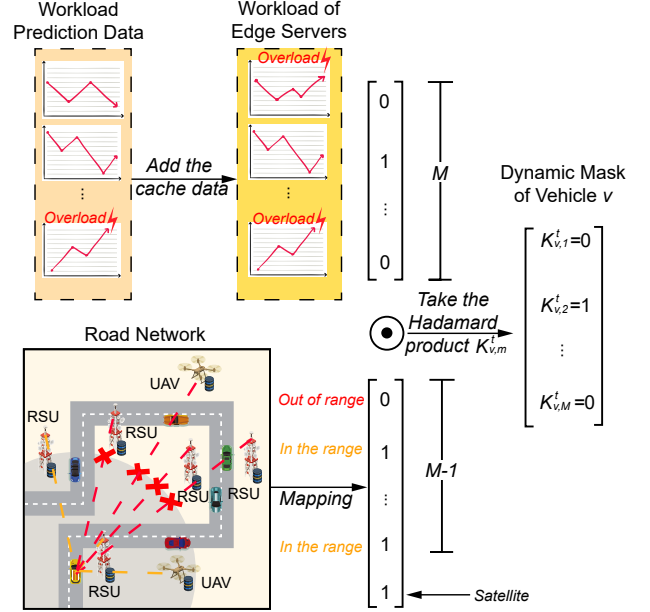


Fig. 4: The structure of the dynamic mask module.

Eq. (21) can be reformulated as

$$r_v^t(\mathbf{o}_v^t, a_v^t) = -(w_T \cdot \tilde{T}_{v,m}^{sum}(t) + w_s \cdot \tilde{S}_m(t) + w_d \cdot \xi_v^t), \quad (22)$$

where $\tilde{S}_m(t)$ denotes the workload of edge server m after Z-score normalization.

- **Dynamic Mask Module:** When VTs of vehicle v migrated to edge server m based on action $a_{v,m}^t$ lead to $S_m^t(t) > L_m^{max}$ or $D_{v,m}(t) > D_m^{max}$ in time slot t , the action $a_{v,m}^t$ are infeasible. We define the infeasible action set as $\mathcal{M}_{v,t}^{infeasible}$. To prevent DRL agents from choosing an infeasible action, we utilize the dynamic mask module to set the probability of infeasible actions to 0 [26], [38], which accelerates agents to identify optimal migration routes. We define the mask list $\mathbf{K}_v^t = [K_{v,1}^t, \dots, K_{v,m}^t, \dots, K_{v,M}^t]$, where $K_{v,m}^t$ is given by

$$K_{v,m}^t = \begin{cases} 0, & m \in \mathcal{M}_{v,t}^{infeasible}, \\ 1, & \text{otherwise.} \end{cases}, \quad (23)$$

Thus, the sampled action a_v^t for vehicle v is rewritten as

$$a_v^t = \underset{m}{\operatorname{argmax}}(\mathbf{P}_v^t \mathbf{K}_v^t). \quad (24)$$

Figure 4 shows the complete calculation process of the dynamic mask module. After mapping the output of the LSTM-based Transformer prediction model to workload data, the dynamic mask module will add the task data stored in the cache to obtain the actual workload of edge server m in time slot t . This is because the unfinished task in the last time slot $t-1$ will be stored in the cache. Finally, the dynamic mask module will determine if the edge server is about to be overloaded based on the size of the VT migration task. In addition, to ensure that VTs are not migrated to edge servers too far away, the dynamic

Algorithm 2: DM-MAPPO for VT Migration Routing

```

1 Initialize actor network parameters  $\theta_v$ ,  $\theta_v^{old}$ , and critic
  network parameters  $w_v$ ;
2 Initialize environment  $Env$  and replay buffer  $Buf$ ;
3 for  $Episode = 1, 2, \dots, End$  do
4   Input historical trajectories to the LSTM-based
    Transformer model.
5   Store predicted workloads into  $Buf$ .
6   for  $v = 1, 2, \dots, V$  do
7     for  $t = 0, 1, \dots, t_v^{end}$  do
8       Get the observation  $\tilde{\mathbf{o}}_v^t$  from  $Env$ .
9       Add the predicted workload into  $\tilde{\mathbf{o}}_v^t$  to get
        the observation  $\mathbf{o}_v^t$ .
10      Each agent gets the action from  $\pi_{\theta^{old}}$ 
        according to  $\mathbf{o}_v^t$ .
11      Mask the infeasible action.
12      Get the reward  $r_v^t$  and the next observation
         $\tilde{\mathbf{o}}_v^{t+1}$  from  $Env$ .
13      Store  $\{\mathbf{o}_v^t, \mathbf{o}_v^{t+1}, a_v^t, r_v^t\}$  into  $Buf$ .
14    end
15    Get the reward list  $\{r_v^t\}_{t=0}^{t_v^{end}}$  and the next
      observation list  $\{\mathbf{o}_v^{t+1}\}_{t=0}^{t_v^{end}}$  from  $Buf$ .
16    Calculate the next value list
       $\{Q_{w_v}(\mathbf{o}_v^{t+1}, a_v^{t+1})\}_{t=0}^{t_v^{end}}$  as target.
17    Calculate the value list  $\{Q_{w_v}(\mathbf{o}_v^t, a_v^t)\}_{t=0}^{t_v^{end}}$  as
      value.
18    Calculate the critic network loss as
       $J_v(w) = \text{MSE}(\text{target}, \text{value})$  using Eq. (26).
19    Update  $w_v$  using  $J_v(w)$  according to Eq. (27).
20    Calculate  $\delta \leftarrow \text{target} - \text{value}$ .
21    Calculate  $A_v^\theta \leftarrow \sum_{t=0}^{t_v^{end}} \delta[t] \cdot \gamma^{t-1}$ .
22    Get  $\pi_{\theta^{old}}$  from the actor network.
23    for  $epoch = 1, 2, \dots, end$  do
24      Get  $\pi_\theta$  from the actor network.
25      Calculate ratio according to Eq. (28).
26      Calculate  $J_v^{clip}$  according to Eq. (31).
27      Calculate the actor network loss  $J_v(\theta_v^{old})$ 
        according to Eq. (32).
28      Update  $\theta_v^{old} \leftarrow \theta_v$ .
29      Update  $\theta_v$  using  $J_v(\theta_v)$  according to Eq.
        (33).
30    end
31  end
32 end
33 return the optimal migration decision sequence
     $[a_v^0, a_v^1, \dots, a_v^t, \dots, a_v^t]_{v=1}^V$ .

```

mask module performs the same mask operation on edge servers beyond the maximum service range D_m^{max} .

B. Algorithm Design

PPO is an on-policy algorithm based on the classic Actor-Critic (AC) framework, which significantly reduces the sampling time required for environment interaction by repeat-

edly training on batch-collected data [39]. Furthermore, by constraining the difference between the new policy and the old policy, the PPO algorithm ensures stable policy updates, thereby enhancing learning efficiency and accelerating convergence [40]. In the AC framework, $Q_{w_v}(\mathbf{o}_v^t, a_v^t)$ is used to estimate the reward expectation in the future after the action a_v^t is executed based on observation \mathbf{o}_v^t , and $Q_{w_v}(\mathbf{o}_v^t, a_v^t)$ is

$$Q_{w_v}(\mathbf{o}_v^t, a_v^t) = \gamma Q_{w_v}(\mathbf{o}_v^{t+1}, a_v^{t+1}) + r_v^t(\mathbf{o}_v^t, a_v^t) \approx \sum_{t'=t}^{t_v^{end}} \gamma^{t'-t} r_v^{t'}(\mathbf{o}_v^t, a_v^t), \quad (25)$$

where γ represents the discount factor.

The AC framework leverages the critic network to fit the reward distribution to judge the action quality generated by the actor network. Thus, the loss function of the critic network is denoted as

$$J_v(w) = \frac{1}{t_v^{end}} \sum_{t=0}^{t_v^{end}} \left[-Q_{w_v}(\mathbf{o}_v^t, a_v^t) + \sum_{t'=t}^{t_v^{end}} \gamma^{t'-t} r_v^{t'}(\mathbf{o}_v^t, a_v^t) \right]^2, \quad (26)$$

and the parameters of the critic network w_v are updated as

$$w_v = w_v + \alpha_w \nabla_w J_v(w). \quad (27)$$

where α_w and $\nabla_w J_v(w)$ represent the learning rate and gradient of the critic network, respectively.

PPO algorithms limit the update rate to ensure that the deviation is within a limited range and define the proportion of the change in the action probability distribution as

$$\text{ratio} = \frac{\pi_\theta(a_v^t | \mathbf{o}_v^t)}{\pi_{\theta^{old}}(a_v^t | \mathbf{o}_v^t)}. \quad (28)$$

To eliminate the influence of positive and negative rewards on the probability of action exploration, the advantage function on the output of the critic network can be calculated as

$$A_v^\theta(\mathbf{o}_v^t, a_v^t) = Q_{w_v}(\mathbf{o}_v^t, a_v^t) - b_{w_v}(\mathbf{o}_v^t), \quad (29)$$

where the baseline $b_{w_v}(\mathbf{o}_v^t)$ is the expected reward for all actions taken at the observation \mathbf{o}_v^t , which is calculated as

$$b_{w_v}(\mathbf{o}_v^t) = \mathbb{E}_{a_v^t \in \mathcal{A}_v^t} [Q_{w_v}(\mathbf{o}_v^t, a_v^t) | \mathbf{o}_v^t], \quad (30)$$

where \mathcal{A}_v^t represents the set of all actions of vehicle v in time slot t , and $\mathbb{E}_{a_v^t \in \mathcal{A}_v^t}[\cdot]$ denotes the expected value.

In addition, the updated range is limited to $(1 - \epsilon, 1 + \epsilon)$, which is calculated as

$$J_v^{clip} = \text{clip}(\text{ratio}, 1 - \epsilon, 1 + \epsilon) \cdot A_v^\theta(\mathbf{o}_v^t, a_v^t). \quad (31)$$

Therefore, the loss function of the actor network can be denoted as [39]

$$J_v(\theta_v) = \mathbb{E}_t \{ \min [\text{ratio} \cdot A_v^\theta(\mathbf{o}_v^t, a_v^t), J_v^{clip}] \}, \quad (32)$$

and the parameters of the actor network θ_v are updated as

$$\theta_v = \theta_v + \alpha_\theta \nabla_\theta J_v(\theta_v), \quad (33)$$

where α_θ represents the learning rate of the actor network.

Algorithm 1 illustrates the pseudocode of the DM-MAPPO algorithm, whose computational complexity is $\mathcal{O}(End \times V \times t_v^{end} \times (M + end))$, where End represents the number of complete interactions of all agents with the environment, and end represents the training epochs of each actor network.

VII. SIMULATION RESULTS

A. Parameter Settings

We first present the parameter settings for the experiments in the VT migration routing scenario. The scenario is sampled every 30s. All UAVs patrol among RSUs at a speed of 3.7m/s. For the network model, the mean of additive Gaussian white noise σ is set to 0, with a variance of 10 [8]. The vehicle trajectories are obtained from the dataset³, and the traffic flow data are sourced from the dataset⁴. The main parameters used in the experiments are summarized in Table I [8], [41]–[43].

To demonstrate the effectiveness of the proposed LSTM-based Transformer model, we compare it against four baseline models: LSTM, GRU, CNN-GRU, and CNN-LSTM. In both CNN-GRU and CNN-LSTM, the input data is initially processed using a one-dimensional convolution with a kernel size of 1, followed by prediction using GRU or LSTM, respectively [44], [45]. For the LSTM-based Transformer model, considering the factors of training time and prediction accuracy, we set the window of historical data input as $T = 6$ to predict the traffic flow data in the next time slot $t + 1$. In particular, for the LSTM prediction layer, the hidden unit in the LSTM module is set to $d_h = 32$. For the Transformer prediction layer, the number of attention heads is set to $H = 4$, and the dimension of query, key, and value vectors is set to $d_k = 64$.

To demonstrate the effectiveness of the proposed DM-MAPPO algorithm, we compare it with several baseline algorithms, including Multi-Agent Soft Actor-Critic (MASAC), Greedy, and Random algorithms. The Greedy algorithm selects the edge server geographically closest to the vehicle for VT migration. To enhance exploration and avoid infeasible actions, a 10% probability is introduced for randomly selecting a server. The Random algorithm performs VT migration by randomly selecting the next edge server without any optimization or learned strategy.

B. Performance of LSTM-based Transformer Models on Workload Prediction

In Fig. 5, we show the predicted RSU workload curve generated by five different prediction algorithms. Among them, the proposed LSTM-based Transformer model yields a prediction curve that most closely aligns with the actual RSU workload. Figure 5 also shows the error rate of each prediction model in the high-frequency part of the traffic flow data, where the LSTM-based Transformer prediction error is always the smallest, outperforming the other models. As shown in Table II, the proposed model achieves the lowest Root Mean Square

TABLE I: Key Parameter Setting in the Paper.

Hyperparameters	Setting
The number of vehicles (C)	5
The number of UAVs (U)	10
The number of RSUs (N)	68 ~ 84
Migration task size (S_v^{mig})	60 MB
CPU operating frequency of UAVs and RSUs (C_m)	32×10^9 Hz
CPU operating frequency of the satellite (C_s)	80×10^9 Hz
Maximum cache capacity of the edge server (L_m^{max})	300 MB
Vehicle transmitting power (p_v)	1000 W
Uplink bandwidth (B_m^{up})	300 MHz
Downlink bandwidth (B_m^{down})	300 MHz
Maximum service distance of RSU ($D_m^{max}, m \in \mathcal{N}_v^t$)	1200 m
Maximum service distance of UAV ($D_m^{max}, m \in \mathcal{U}_v^t$)	1500 m
UAV cruising altitude (h_u)	50 m
The number of CPU cycles required per unit data (e_v)	1000 cycles/bit

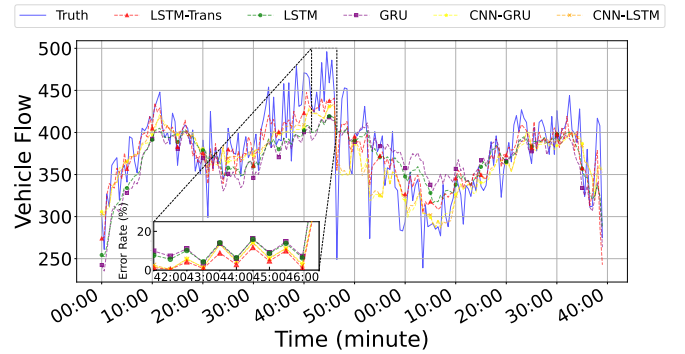


Fig. 5: The workload of edge servers predicted by different prediction algorithms over time.

Error (RMSE) and Mean Absolute Error (MAE), indicating the smallest deviation between the predicted and actual values. Specifically, the proposed LSTM-based Transformer model achieves a prediction error rate of 6.814%, highlighting its superior prediction performance. Moreover, the determination R^2 of the model approaches 1, demonstrating strong explanatory power and the ability to capture most of the variance in the workload data. The LSTM-based Transformer model outperforms all baselines across all four evaluation metrics, This is because LSTM possesses the powerful capability of processing time-series data. By first leveraging LSTM to capture temporal dependencies and reduce high-frequency noise, followed by the self-attention mechanism of Transformer for fine-grained prediction refinement, the model delivers highly accurate results.

C. Performance of DM-MAPPO on VT Migration Routing

1) *Performance of LSTM-based Transformer models for VT migration route planning:* As shown in Fig. 6 (a), we comprehensively evaluate the performance of the proposed DM-MAPPO algorithm with and without the LSTM-based Transformer prediction model. For ease of expression, we

³Vehicle trajectory dataset: <https://www.microsoft.com/en-us/research/publication/t-drive-trajectory-data-sample/>

⁴California traffic flow dataset: <https://pems.dot.ca.gov/>

TABLE II: The Performance of Various Prediction Algorithms.

Metrics	Ours	CNN-GRU	LSTM	GRU	CNN-LSTM
RMSE	0.671	0.812	0.877	0.916	0.917
MAE	20.417	27.802	25.330	29.466	29.461
Error Rate	6.814%	9.451%	8.741%	9.843%	9.796%
R^2	0.925	0.865	0.884	0.851	0.855

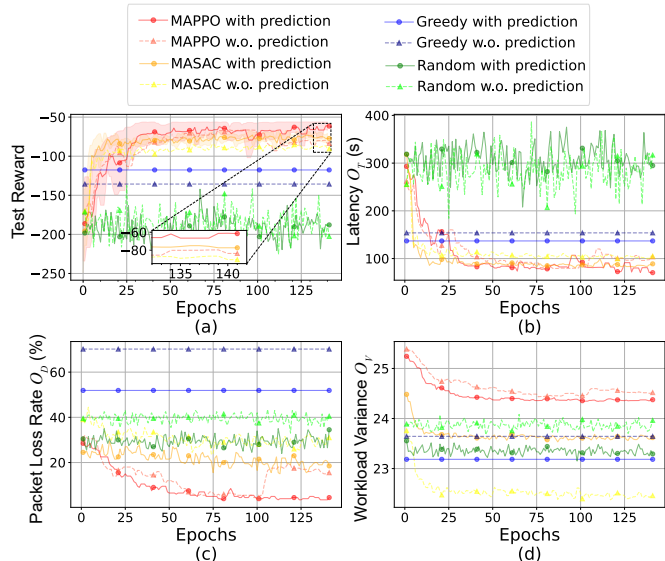


Fig. 6: Performance comparison of test reward curves for various DRL algorithms under the dynamic mask module.

call them *MAPPO with prediction* and *MAPPO w.o. prediction*, respectively. The test reward achieved by *MAPPO with prediction* is 35.99% higher than that of *MAPPO w.o. prediction*. Similarly, the test reward achieved by *MASAC with prediction* is 17.08% higher than that of *MASAC w.o. prediction*. The above results indicate that the integration of the LSTM-based Transformer model significantly reduces the likelihood of infeasible actions taken by the DM-MAPPO algorithm. In Fig. 6 (b), the total latency $T_{v,m}^{sum}(t)$ achieved by *MAPPO with prediction* is 70.4729 s, which corresponds to an average transmission latency of 8.42 ms per vehicle per data transmission. This is lower than the 12.40 ms latency obtained using *MAPPO w.o. prediction*. Furthermore, Fig. 6 (c) shows that *MAPPO with prediction* achieves the lowest packet loss rate of 4.494%, ensuring a high-quality immersive experience. In terms of workload balancing, Fig. 6 (d) shows that *MAPPO with prediction* reduces the workload variance of the edge server cluster to 24.38, and *MAPPO w.o. prediction* to 24.53, which proves that the LSTM-based Transformer model can balance the workload. This shows that our proposed *MAPPO with prediction* effectively reduces transmission delay and packet loss while improving workload distribution, enhancing the overall immersive experience for users.

2) *Performance of DM-MAPPO on various VT migration tasks*: As shown in Fig. 7, the test reward of each algorithm decreases as the migration data increases. This is due to

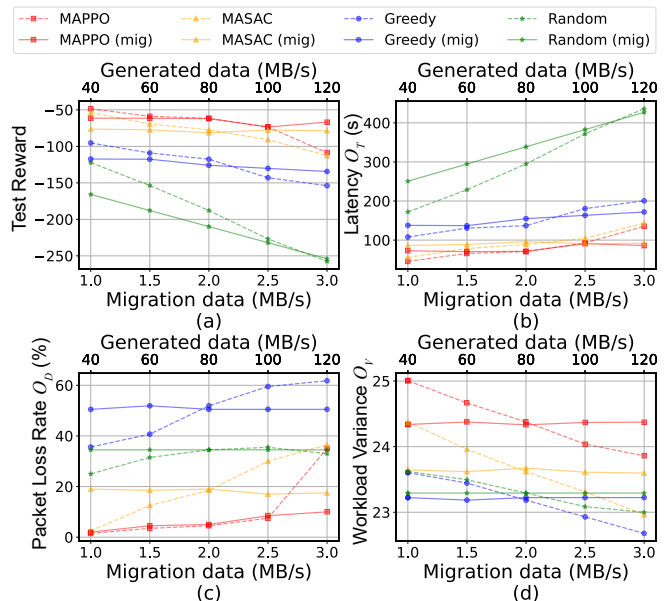


Fig. 7: Performance comparison of different DRL algorithms in multiple evaluation metrics, including test rewards, latency, packet loss rates, and variances of workloads.

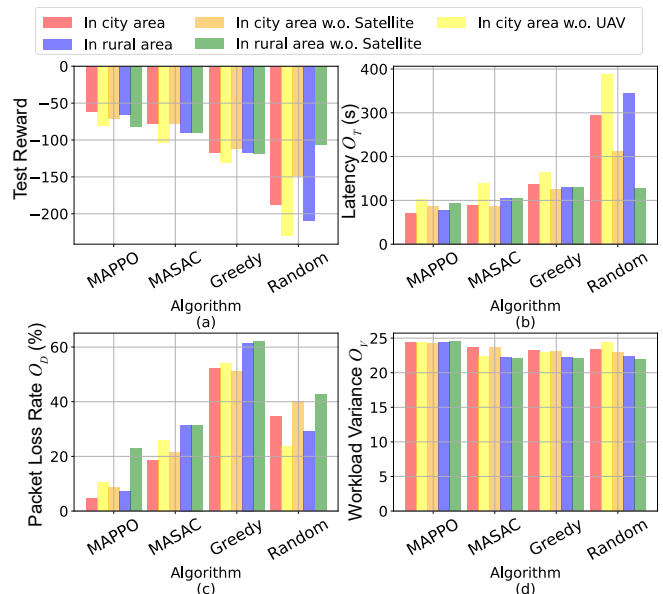


Fig. 8: The ablation of different framework elements.

the inevitable increase in computation and communication times caused by larger migration data packets. For migration data rates of 40 MB/s, 60 MB/s, 80 MB/s, 100 MB/s, and 120 MB/s, our proposed DM-MAPPO algorithm consistently achieves the lowest latency and packet loss rate, as shown in Fig. 7 (b) and Fig. 7 (c). Specifically, when the migration data rate is at or below 100 MB/s, the packet loss rate of DM-MAPPO remains below 10%, indicating that the proposed DM-MAPPO algorithm ensures stable and reliable data transmission during VT migration. Furthermore, to assess the impact of varying computational requirements, we conduct

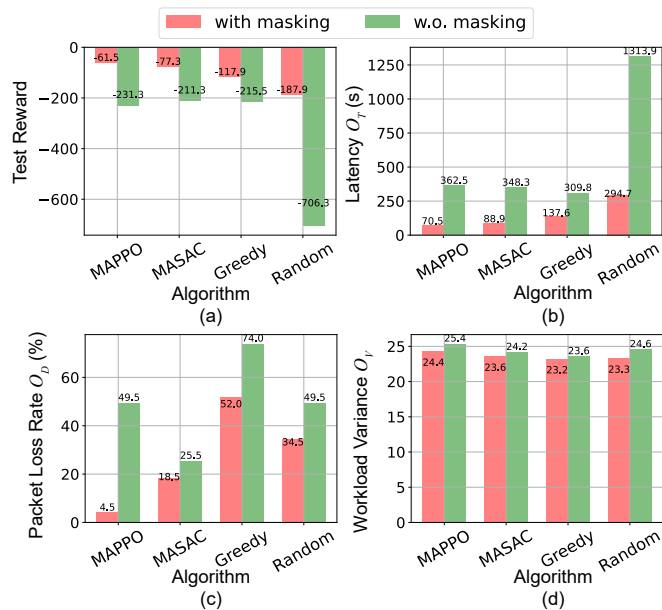


Fig. 9: Comparison of performance gains brought by the dynamic mask module.

experiments with tasks that generate different volumes of data. In Fig. 7 (d), the workload variance decreases with the increase of generated data. This is because each vehicle can cause a greater impact on the edge server network. Thus, when serving vehicles, the workload of edge servers with low workloads will be increased, and the workload variance will be reduced. For generated data rates of 1.0 MB/s, 1.5 MB/s, 2.0 MB/s, 2.5 MB/s, and 3.0 MB/s, our proposed DM-MAPPO can achieve the lowest latency and packet loss rate, which demonstrates that DM-MAPPO can reasonably migrate VTs under different computational task requirements to minimize both total latency and packet loss.

3) *Ablation study on framework elements*: We conduct an ablation study by independently removing UAVs and the satellite from the proposed framework to evaluate their respective contributions to VT migration. As shown in Fig. 8, in the city area without UAVs, the test reward of the four algorithms decreases by an average of 6.90%, while the average latency and packet loss rate increase by 37.88% and 29.78%, respectively. The reason is that when RSUs are overloaded, VTs can be migrated to UAVs, avoiding a complete interruption of vehicular services, which indicates that UAVs can alleviate the uneven distribution of RSUs and the problem of insufficient computing resources during peak hours in the city area. In addition, in the city area, DM-MAPPO can further reduce the latency and packet loss rate of VT migration with satellites, while the performance of all baseline algorithms declines with satellite due to the high cost of satellite communication, resulting in high latency and packet loss rates. Compared with the city area, the performance of each algorithm decreases in the rural area environment. Fortunately, in rural areas with satellites, the latency and packet loss rates of VT migration are lower than in rural areas without satellites, suggesting that satellites can compensate for the lack of RSU support for

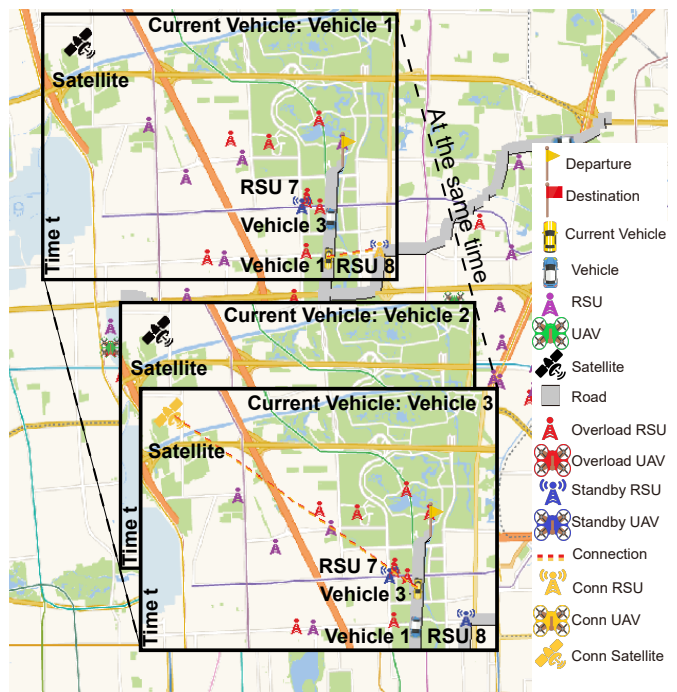


Fig. 10: Cooperative behavior exhibited by multiple PPO agents when planning multiple VT migration routes in the same area.

communication services in remote areas.

4) *Ablation study on the effectiveness of the dynamic mask module*: To assess the performance improvement brought by the dynamic mask module for each algorithm, we conduct an ablation study by removing this module from four algorithms, allowing VTs to be migrated to any edge server without constraints. As shown in Fig. 9, algorithms with the masking module significantly outperform those without the masking module in terms of latency and packet loss rates, with an average latency reduction of 72.05% and an average packet loss rate reduction of 44.60%. Particularly, the dynamic mask module brings a 73.41% performance improvement to MAPPO, enabling it to surpass MASAC. Moreover, the dynamic mask module can reduce workload variance, balancing the workload of RSUs in the region.

5) *Visual Analysis of multi-agent cooperative behavior*: To demonstrate the cooperation among agents in DM-MAPPO during the VT migration process, we develop a visualization platform to display the migration of each VT intuitively. As shown in Fig. 10, in time slot t , both vehicle 1 and vehicle 3 are traveling from north to south within the same region. As they approach the coverage boundary of RSU 7, they need to migrate their VTs to edge servers with better channel quality, thus ensuring the immersion of VT services. For vehicle 1, RSU 8, and the satellite are identified as feasible edge server targets for VT migration. Given the higher communication cost associated with satellite links, vehicle 1 opts to migrate its VTs to RSU 8. Since the agents in DM-MAPPO share information such as workload information, vehicle 3 migrating its VTs to RSU 8 will overload RSU 8, which may cause packet loss and affect the VT services of other vehicles. Therefore, for

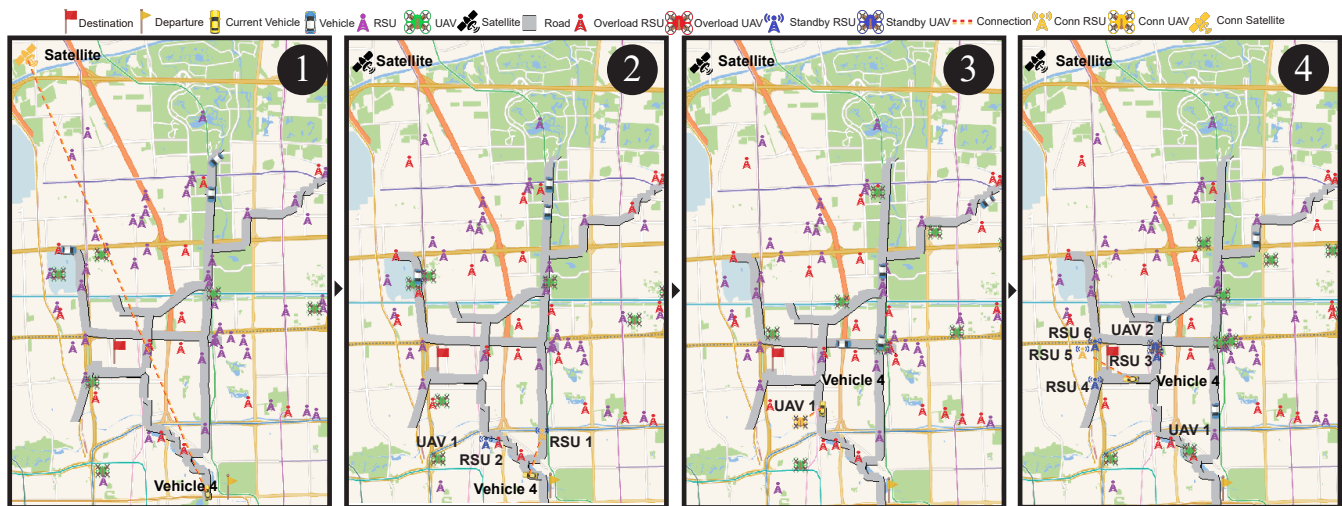


Fig. 11: Single VT migration process in real scenarios.

vehicle 3, migrating its VTs to the satellite can maximize the overall benefit for all vehicles, which shows that our proposed DM-MAPPO can solve cooperative tasks well.

6) *Visual analysis of the VT migration process:* In Fig. 11, we present the complete VT migration trajectory of vehicle 4 within the target region. At moment 1, there are no RSUs or UAVs in the standby state. Therefore, the optimal option for vehicle 4 is to migrate its VTs to the satellite. At moment 2, vehicle 4 enters the service range of RSU 1 and RSU 2. To avoid the high costs of satellite services, the vehicle 4 migrates its VTs from the satellite to the RSU 1. At moment 3, RSU 2 is overloaded, and vehicle 4 is out of the service range of RSU 1 but enters the service range of UAV 1. Since the communication costs for UAVs are significantly lower than those for the satellite, the optimal option for vehicle 4 is to migrate its VTs to UAV 1. At moment 4, vehicle 4 is out of the service range of UAV 1 and migrates its VTs to RSU 5. This is because RSU 5 is the closest RSU to the destination, and vehicle 4 does not need to migrate VTs again, which can minimize total latency. This indicates that the actions taken by our proposed DM-MAPPO are highly interpretable, the migration process is clear, and the planned VT migration path is reasonable and reliable.

VIII. CONCLUSION

In this paper, we have addressed the challenges of optimizing multi-objective VT migration routing in 6G-enabled IoV networks. Specifically, we have proposed a workload prediction-based VT migration framework that leverages a heterogeneous edge server architecture comprising RSUs, UAVs, and the satellite. This architecture is particularly effective in mitigating the problem of low resource utilization in sparsely distributed regions. To enable accurate long-term workload prediction, we have proposed the LSTM-based Transformer model that integrates the LSTM module into the Transformer model. Furthermore, we have proposed the DM-MAPPO algorithm based on the dynamic mask module to facilitate efficient VT migration route planning in complex environments. The

DM-MAPPO algorithm can greatly reduce the probability of infeasible actions and comprehensively optimize key performance metrics such as latency, packet loss rate, and regional workload balance. Simulation results have demonstrated that the LSTM-based Transformer model can reduce the error rate to 6.814%, achieving accurate traffic flow prediction, and the performance of the DM-MAPPO algorithm has been improved by 73.41% compared with MAPPO. For future work, since our current framework considers all edge servers to be fully trustworthy, which may lead to the potential exposure of VT migration data and vehicle trajectories, we will explore the integration of privacy-preserving mechanisms into our framework.

REFERENCES

- [1] X. Zhou, M. Bilal, R. Dou, J. J. P. C. Rodrigues, Q. Zhao, J. Dai, and X. Xu, "Edge Computation Offloading With Content Caching in 6G-Enabled IoV," *IEEE Transactions on Intelligent Transportation Systems*, vol. 25, no. 3, pp. 2733–2747, 2024.
- [2] W. Saad, M. Bennis, and M. Chen, "A Vision of 6G Wireless Systems: Applications, Trends, Technologies, and Open Research Problems," *IEEE Network*, vol. 34, no. 3, pp. 134–142, 2020.
- [3] H. Guo, J. Li, J. Liu, N. Tian, and N. Kato, "A Survey on Space-Air-Ground-Sea Integrated Network Security in 6G," *IEEE Communications Surveys & Tutorials*, vol. 24, no. 1, pp. 53–87, 2022.
- [4] Y. Wang, Z. Su, N. Zhang, R. Xing, D. Liu, T. H. Luan, and X. Shen, "A Survey on Metaverse: Fundamentals, Security, and Privacy," *IEEE Communications Surveys & Tutorials*, vol. 25, no. 1, pp. 319–352, 2023.
- [5] M. Xu, W. C. Ng, W. Y. B. Lim, J. Kang, Z. Xiong, D. Niyato, Q. Yang, X. Shen, and C. Miao, "A Full Dive Into Realizing the Edge-Enabled Metaverse: Visions, Enabling Technologies, and Challenges," *IEEE Communications Surveys & Tutorials*, vol. 25, no. 1, pp. 656–700, 2023.
- [6] Y. Kang, J. Wen, J. Kang, T. Zhang, H. Du, D. Niyato, R. Yu, and S. Xie, "Hybrid-Generative Diffusion Models for Attack-Oriented Twin Migration in Vehicular Metaverses," *arXiv preprint arXiv:2407.11036*, 2024.
- [7] Y. Dai and Y. Zhang, "Adaptive Digital Twin for Vehicular Edge Computing and Networks," *Journal of Communications and Information Networks*, vol. 7, no. 1, pp. 48–59, 2022.
- [8] J. Chen, J. Kang, M. Xu, Z. Xiong, D. Niyato, C. Chen, A. Jamalipour, and S. Xie, "Multiagent Deep Reinforcement Learning for Dynamic Avatar Migration in AIoT-Enabled Vehicular Metaverses With Trajectory Prediction," *IEEE Internet of Things Journal*, vol. 11, no. 1, pp. 70–83, 2024.

- [9] J. Wen, J. Nie, Y. Zhong, C. Yi, X. Li, J. Jin, Y. Zhang, and D. Niyato, "Diffusion-Model-Based Incentive Mechanism With Prospect Theory for Edge AIGC Services in 6G IoT," *IEEE Internet of Things Journal*, vol. 11, no. 21, pp. 34 187–34 201, 2024.
- [10] L. Chen, B. Hu, Z.-H. Guan, L. Zhao, and X. Shen, "Multiagent Meta-Reinforcement Learning for Adaptive Multipath Routing Optimization," *IEEE Transactions on Neural Networks and Learning Systems*, vol. 33, no. 10, pp. 5374–5386, 2022.
- [11] W. Song, S. Rajak, S. Dang, R. Liu, J. Li, and S. Chinnadurai, "Deep Learning Enabled IRS for 6G Intelligent Transportation Systems: A Comprehensive Study," *IEEE Transactions on Intelligent Transportation Systems*, vol. 24, no. 11, pp. 12 973–12 990, 2023.
- [12] J. Guo, M. Bilal, Y. Qiu, C. Qian, X. Xu, and K.-K. Raymond Choo, "Survey on Digital Twins for Internet of Vehicles: Fundamentals, Challenges, and Opportunities," *Digital Communications and Networks*, vol. 10, no. 2, pp. 237–247, 2024.
- [13] X. Xu, Q. Jiang, P. Zhang, X. Cao, M. R. Khosravi, L. T. Alex, L. Qi, and W. Dou, "Game Theory for Distributed IoV Task Offloading With Fuzzy Neural Network in Edge Computing," *IEEE Transactions on Fuzzy Systems*, vol. 30, no. 11, pp. 4593–4604, 2022.
- [14] T. Z. H. Ernest and A. S. Madhukumar, "Computation Offloading in MEC-Enabled IoV Networks: Average Energy Efficiency Analysis and Learning-Based Maximization," *IEEE Transactions on Mobile Computing*, vol. 23, no. 5, pp. 6074–6087, 2024.
- [15] M. H. Adnan, Z. A. Zukarnain, and O. A. Amodu, "Fundamental Design Aspects of UAV-enabled MEC Systems: A Review on Models, Challenges, and Future Opportunities," *Computer Science Review*, vol. 51, p. 100615, 2024.
- [16] X. Yuan, W. Zhang, J. Yang, M. Xu, D. Niyato, Q. Deng, and C. Li, "Efficient IoV Resource Management Through Enhanced Clustering, Matching, and Offloading in DT-Enabled Edge Computing," *IEEE Internet of Things Journal*, vol. 11, no. 18, pp. 30 172–30 186, 2024.
- [17] T. Liu, L. Tang, W. Wang, X. He, Q. Chen, X. Zeng, and H. Jiang, "Resource Allocation in DT-assisted Internet of Vehicles via Edge Intelligent Cooperation," *IEEE Internet of Things Journal*, vol. 9, no. 18, pp. 17 608–17 626, 2022.
- [18] Z. Chen, M. Ma, T. Li, H. Wang, and C. Li, "Long Sequence Time-series Forecasting with Deep Learning: A Survey," *Information Fusion*, vol. 97, p. 101819, 2023.
- [19] G. ALMahadin, Y. Aoudni, M. Shabaz, A. V. Agrawal, G. Yasmin, E. S. Alomari, H. M. R. Al-Khafaji, D. Dansana, and R. R. Maaliw, "VANET Network Traffic Anomaly Detection Using GRU-Based Deep Learning Model," *IEEE Transactions on Consumer Electronics*, vol. 70, no. 1, pp. 4548–4555, 2024.
- [20] J. Sun, X. Zhang, and J. Wang, "Lightweight Bidirectional Long Short-term Memory Based on Automated Model Pruning with Application to Bearing Remaining Useful Life Prediction," *Engineering Applications of Artificial Intelligence*, vol. 118, p. 105662, 2023.
- [21] F. Li, J. Feng, H. Yan, G. Jin, F. Yang, F. Sun, D. Jin, and Y. Li, "Dynamic Graph Convolutional Recurrent Network for Traffic Prediction: Benchmark and Solution," *ACM Trans. Knowl. Discov. Data*, vol. 17, no. 1, Feb. 2023.
- [22] H. Zhou, J. Li, S. Zhang, S. Zhang, M. Yan, and H. Xiong, "Expanding the Prediction Capacity in Long Sequence Time-series Forecasting," *Artificial Intelligence*, vol. 318, p. 103886, 2023.
- [23] S. Liu, H. Yu, C. Liao, J. Li, W. Lin, A. X. Liu, and S. Dustdar, "Pyraformer: Low-Complexity Pyramidal Attention for Long-Range Time Series Modeling and Forecasting," in *The Tenth International Conference on Learning Representations (ICLR 2022)*, 2022.
- [24] H. Zhou, S. Zhang, J. Peng, S. Zhang, J. Li, H. Xiong, and W. Zhang, "Informer: Beyond Efficient Transformer for Long Sequence Time-Series Forecasting," *Proceedings of the AAAI Conference on Artificial Intelligence*, vol. 35, no. 12, pp. 11 106–11 115, May 2021.
- [25] B. Mao, X. Zhou, J. Liu, and N. Kato, "On a Cooperative Deep Reinforcement Learning-Based Multi-Objective Routing Strategy for Diversified 6G Metaverse Services," *IEEE Transactions on Vehicular Technology*, vol. 73, no. 9, pp. 14 092–14 096, 2024.
- [26] H. Kang, X. Chang, J. Mišić, V. B. Mišić, J. Fan, and Y. Liu, "Cooperative UAV Resource Allocation and Task Offloading in Hierarchical Aerial Computing Systems: A MAPPO-Based Approach," *IEEE Internet of Things Journal*, vol. 10, no. 12, pp. 10 497–10 509, 2023.
- [27] X. Ning, M. Zeng, M. Hua, and Z. Fei, "Multiple Reconfigurable Intelligent Surfaces Aided Vehicular Edge Computing Networks: A MAPPO-Based Approach," *IEEE Transactions on Vehicular Technology*, vol. 73, no. 11, pp. 17 496–17 509, 2024.
- [28] D. Zhong, Y. Yang, and Q. Zhao, "No Prior Mask: Eliminate Redundant Action for Deep Reinforcement Learning," in *Proceedings of the AAAI Conference on Artificial Intelligence*, vol. 38, no. 15, 2024, pp. 17 078–17 086.
- [29] J. Wen, J. Kang, Z. Xiong, Y. Zhang, H. Du, Y. Jiao, and D. Niyato, "Task Freshness-Aware Incentive Mechanism for Vehicle Twin Migration in Vehicular Metaverses," in *2023 IEEE International Conference on Metaverse Computing, Networking and Applications (MetaCom)*, 2023, pp. 481–487.
- [30] C. E. Shannon, "A Mathematical Theory of Communication," *The Bell System Technical Journal*, vol. 27, no. 3, pp. 379–423, 1948.
- [31] P. Ren, X. Qiao, Y. Huang, L. Liu, C. Pu, S. Dustdar, and J. Chen, "Edge AR X5: An Edge-Assisted Multi-User Collaborative Framework for Mobile Web Augmented Reality in 5G and Beyond," *IEEE Transactions on Cloud Computing*, vol. 10, no. 4, pp. 2521–2537, 2022.
- [32] H. Yadav and A. Thakkar, "NOA-LSTM: An Efficient LSTM Cell Architecture for Time Series Forecasting," *Expert Systems with Applications*, vol. 238, p. 122333, 2024.
- [33] A. Khan, M. M. Fouda, D.-T. Do, A. Almaleh, and A. U. Rahman, "Short-Term Traffic Prediction Using Deep Learning Long Short-Term Memory: Taxonomy, Applications, Challenges, and Future Trends," *IEEE Access*, vol. 11, pp. 94 371–94 391, 2023.
- [34] A. Vaswani, "Attention is all you need," *Advances in Neural Information Processing Systems*, 2017.
- [35] B. Gülmez, "Stock Price Prediction with Optimized Deep LSTM Network with Artificial Rabbits Optimization Algorithm," *Expert Systems with Applications*, vol. 227, p. 120346, 2023.
- [36] S. A. Cook, "The Complexity of Theorem-Proving Procedures," in *Logic, automata, and computational complexity: The works of Stephen A. Cook*, 2023, pp. 143–152.
- [37] Y. Hu, W. Wang, H. Jia, Y. Wang, Y. Chen, J. Hao, F. Wu, and C. Fan, "Learning to Utilize Shaping Rewards: A New Approach of Reward Shaping," in *Advances in Neural Information Processing Systems*, H. Larochelle, M. Ranzato, R. Hadsell, M. Balcan, and H. Lin, Eds., vol. 33. Curran Associates, Inc., 2020, pp. 15 931–15 941.
- [38] J. Wen, J. Kang, D. Niyato, Y. Zhang, and S. Mao, "Sustainable Diffusion-Based Incentive Mechanism for Generative AI-Driven Digital Twins in Industrial Cyber-Physical Systems," *IEEE Transactions on Industrial Cyber-Physical Systems*, vol. 3, pp. 139–149, 2025.
- [39] J. Schulman, F. Wolski, P. Dhariwal, A. Radford, and O. Klimov, "Proximal Policy Optimization Algorithms," *CoRR*, vol. abs/1707.06347, 2017.
- [40] J. Kang, Y. Zhong, M. Xu, J. Nie, J. Wen, H. Du, D. Ye, X. Huang, D. Niyato, and S. Xie, "Tiny multiagent DRL for twins migration in UAV metaverses: A multileader multi-follower stackelberg game approach," *IEEE Internet of Things Journal*, vol. 11, no. 12, pp. 21 021–21 036, 2024.
- [41] E. Dinc, M. Vondra, and C. Cavdar, "Total Cost of Ownership Optimization for Direct Air-to-Ground Communication Networks," *IEEE Transactions on Vehicular Technology*, vol. 70, no. 10, pp. 10 157–10 172, 2021.
- [42] A. Masaracchia, Y. Li, K. K. Nguyen, C. Yin, S. R. Khosravirad, D. B. D. Costa, and T. Q. Duong, "UAV-Enabled Ultra-Reliable Low-Latency Communications for 6G: A Comprehensive Survey," *IEEE Access*, vol. 9, pp. 137 338–137 352, 2021.
- [43] J. Wang, D. Feng, S. Zhang, J. Tang, and T. Q. S. Quek, "Computation Offloading for Mobile Edge Computing Enabled Vehicular Networks," *IEEE Access*, vol. 7, pp. 62 624–62 632, 2019.
- [44] P. T. Yamak, L. Yujian, and P. K. Gadosey, "A Comparison Between ARIMA, LSTM, and GRU for Time Series Forecasting," in *Proceedings of the 2019 2nd International Conference on Algorithms, Computing and Artificial Intelligence*, ser. ACAI '19. New York, NY, USA: Association for Computing Machinery, 2020, p. 49–55.
- [45] H. Song and H. Choi, "Forecasting Stock Market Indices Using the Recurrent Neural Network Based Hybrid Models: CNN-LSTM, GRU-CNN, and Ensemble Models," *Applied Sciences*, vol. 13, no. 7, 2023.